Inorg. Chem. **2003**, *42*, 8203–8213

$[Mn_2(saltmen)_2Ni(pao)_2(L)_2](A)_2$ with L = Pyridine, 4-Picoline, 4-*tert*-Butylpyridine, *N*-Methylimidazole and A = ClO_4^-, BF_4^-, PF_6^-, ReO_4^-: A Family of Single-Chain Magnets

Hitoshi Miyasaka,*[,†,‡] Rodolphe Clérac,*[,§] Kaori Mizushima,[†] Ken-ichi Sugiura,[†] Masahiro Yamashita,[†] Wolfgang Wernsdorfer,[||] and Claude Coulon[§]

Department of Chemistry, Graduate School of Science, Tokyo Metropolitan University, 1-1 Minami-ohsawa, Hachioji, Tokyo 192-0397, Japan, "Structural Ordering and Physical Properties", PRESTO, Japan Science and Technology Agency, 4-1-8 Honcho Kawaguchi, Saitama 332-0012, Japan, Centre de Recherche Paul Pascal, CNRS UPR 8641, 115 Avenue du Dr. A. Schweitzer, 33600 Pessac, France, and Laboratoire Louis Néel, CNRS, BP 166, 25 Avenue des Martyrs, 38042 Grenoble Cedex 9, France

Received July 24, 2003

A series of single-chain magnets, $[Mn_2(saltmen)_2Ni(pao)_2(L)_2](A)_2$ (saltmen^{2-} = *N*,*N*′-(1,1,2,2-tetramethylethylene) bis(salicylideneiminate), pao$^-$ = pyridine-2-aldoximate; A$^-$ = ClO_4^- with L = 4-picoline; **2**, 4-*tert*-butylpyridine; **3**, *N*-methylimidazole; **4**, and L = pyridine with A$^-$ = BF_4^-; **5**, PF_6^-; **6**, ReO_4^-; **7**), was prepared by reactions between Mn^{III} dimer units, i.e., $[Mn_2(saltmen)_2(H_2O)_2](A)_2$ (A$^-$ = ClO_4^-, BF_4^-, PF_6^-) or $Mn_2(saltmen)_2(ReO_4)_2$, and Ni^{II} monomeric units, i.e., $Ni(pao)_2(L)_2$, in methanol/water media. The crystal structures of **4**, **6**, and **7** were established by single-crystal X-ray crystallography. These three compounds are isostructural with $[Mn_2(saltmen)_2Ni(pao)_2(py)_2](ClO_4)_2$ (**1**) (Clérac, R.; Miyasaka, H.; Yamashita, M.; Coulon, C. *J. Am. Chem. Soc.* **2002**, *124*, 12837) and crystallize in monoclinic space group *C*2/*c*. The linear arrangement of Mn^{III} dimer units and Ni^{II} building blocks leads to an alternating chain having a repeating unit, [–$(O)_2$–Mn–ON–Ni–NO–Mn–]. The chains are well separated with the nearest interchain intermetallic distance of 10.36 Å for **4**, 10.51 Å for **6**, and 10.30 Å for **7**, and there is no significant π–π interchain interaction between ligands. The void space between the chains is occupied by counteranions, which control the three-dimensional organization of the chains. The X-ray diffraction analysis (XRD) on a powder sample was also performed for all compounds. The XRD patterns for **1**, **2**, and **4**–**7** are very similar, emphasizing the isostructural nature of these materials although they have individually slight different interchain distances. Inversely, the XRD pattern for **3** reveals a completely different shape being indicative of the peculiar crystal packing compared to the others. Nevertheless, the one-dimensional nature of the structure is also kept in **3** as indicated by magnetic measurements. The whole family of compounds exhibits quasi-identical magnetic behavior compared to that described for **1**. Above 30 K, the heterometallic chain can be described as an assembly of antiferromagnetically coupled Mn···Ni···Mn trimers (via oximate bridge, $-24.2\ K < J_{Mn-Ni}/k_B < -20.8\ K$) connected through Mn···Mn ferromagnetic interaction (via the phenolate bridge, $J_{Mn-Mn}/k_B \approx +0.7$ K), assuming a ferromagnetic chain with $S = 3$ units. In the low temperature region, combined ac and dc magnetic measurements revealed for the whole series the systematic presence of a magnet behavior exhibiting coercivity and slow relaxation of magnetization below 3.5 K. This behavior was analyzed on the basis of Glauber's theory for an Ising one-dimensional system which predicts an activated dependence (Arrhenius law) of the relaxation time: $\tau = \tau_0 \exp(\Delta/k_BT)$. Similar values of $\tau_0 \approx 1 \times 10^{-10}$ s and $\Delta/k_B \approx 70$ K have been found along the series. The described compounds constitute the first example of the rational design of a single-chain magnet family and clearly demonstrate the unique behavior of these heterometallic chains independently of their interchain environments.

Introduction

The design of new magnetic materials based on molecules is still one of the most important research subjects for chemistry and physics communities. In the 1990s, a large variety of molecule-based magnetic materials were synthe-

* To whom correspondence should be addressed. E-mail: miyasaka@comp.metro-u.ac.jp (H.M.); clerac@crpp-bordeaux.cnrs.fr (R.C.). Fax: (+81) 426-77-2525 (H.M.); (+33) 5-56-84 56 00 (R.C.).

† Tokyo Metropolitan University.
‡ PRESTO, JST.
§ Centre de Recherche Paul Pascal.
|| Laboratoire Louis Néel.

10.1021/ic034872o CCC: $25.00
Published on Web 11/06/2003

sized over the years with a fine-tuning of local exchange interaction between spin carriers using appropriate bridging ligands and with synthetic control of their bulk magnetic properties, e.g., coercivity, critical temperature, and remnant magnetization. The more usual way to obtain a magnet is the synthesis of materials containing strong three-dimensional magnetic couplings between spin carriers, which lead to ferro- or ferrimagnets. Another possible way for constructing a magnet is the use of paramagnetic or superparamagnetic systems presenting slow relaxation of their magnetization. The global magnetization of these materials relaxes to zero with a characteristic time (τ). With lowering temperature, this time becomes longer and longer and finally reaches a characteristic time (τ_{exp}) which becomes experimentally detectable. This crossover ($\tau_{exp} = \tau$) is thus achieved at the blocking temperature (T_B). At lower temperatures ($T \ll T_B$), τ might be able to reach years, and the material can be therefore considered as a magnet. The most well-known example of this type of magnetic behavior is a family of superparamagnetic molecular clusters (e.g., Mn_{12}, Mn_4, Fe_8, Fe_4, and so forth), so-called single-molecule magnets (SMMs).[1−8] In their crystal structures, the magnetic entities are generally well isolated by bulky ligands, and hence, the dynamics of these materials results from the slow relaxation of individual cluster spins (S). The slow dynamics, deeply associated with the combined effects of a high spin ground state value (S), uniaxial anisotropy ($D < 0$; D is defined as the zero-field splitting parameter) of the cluster, and small transverse anisotropy terms, follows an activated Arrhenius law with a characteristic energy gap Δ for reversal between up-spin and down-spin given roughly by $\Delta = |D|S^2$. The slow relaxation behavior is observed at low temperature when $|D|S^2 \gg k_BT$. Another type of magnets has recently been described in the literature for one-dimensional systems.[9,10] By analogy to the SMM behavior, this type of material has been called a single-chain magnet (SCM).[9] In such a system, the slow relaxation of the magnetization is not caused by isolated anisotropic entities, namely those like SMMs, which would individually relax slowly, but by the introduction of magnetic interactions between fast relaxing units. Therefore, slowing down of the relaxation can also be understood as the result of magnetic correlation. In the one-dimensional case, the development of short-range order is induced along the chain in a large temperature domain as a critical point is quite generally located at 0 K. In the special case of Ising systems, the dynamics has been exactly described by R. J. Glauber in 1963, using a stochastic approach.[11] He predicted the presence of the slow relaxation of the magnetization on a chain composed of ferromagnetically coupled Ising spins.[11,12] This work suggests that a material composed of this type of chain, which are individually magnetically isolated, could be a magnet. To design this kind of material, four different ingredients need to be considered. First, the magnetic unit of the chain needs to possess a spin ground state (S) with a uniaxial anisotropy (Ising-like) to be able to block its magnetization along an easy axis. Moreover, these high spin magnetic units need to be coupled along the chain in such way that they do not compensate. At the same time, the magnetic interchain interactions need to be weak in order to avoid the stabilization of three-dimensional magnetic order. In 2001, A. Caneschi et al. reported the first experimental evidence of SCM behavior in a ferrimagnetic chain, $Co^{II}(hfac)_2$(NITPhOMe) (hfac = hexafluoroacetylacetonate, NITPhOMe = 4′-methoxy-phenyl-4,4,5,5-tetramethylimidazoline-1-oxyl-3-oxide).[10] This compound consists of $Co(hfac)_2$ and NITPhOMe radical moieties alternately arranged in a helical

(1) Gatteschi, D.; Sessoli, R. *Angew. Chem., Int. Ed.* **2003**, *42*, 268−297.

(2) (a) Sessoli, R.; Tsai, H.-L.; Schake, A. R.; Wang, S.; Vincent, J. B.; Folting, K.; Gatteschi, D.; Christou, G.; Hendrickson, D. N. *J. Am. Chem. Soc.* **1993**, *115*, 1804−1816. (b) Gatteschi, D.; Caneschi, A.; Pardi, L.; Sessoli, R. *Science* **1994,** *265*, 1054−1058. (c) Eppley, H. J.; Tsai, H.-L.; de Vries, N.; Folting, K.; Christou, G.; Hendrickson, D. N. *J. Am. Chem. Soc.* **1995**, *117*, 301−317. (d) Aromi, G.; Aubin, S. M. J.; Bolcar, M. A.; Christou, G.; Eppley, H. J.; Folting, K.; Hendrickson, D. N.; Huffman, J. C.; Squire, R. C.; Tsai, H.-L.; Wang, S.; Temple, M. W. *Polyhedron* **1998**, *17*, 3005−3020. (e) Barra, A.-L.; Brunel, L.-C.; Gatteschi, D.; Pardi, L.; Sessoli, R. *Acc. Chem. Res.* **1998**, *31*, 460−466. (f) Goodwin, J. C.; Sessoli, R.; Gatteschi, D.; Wernsdorfer, W.; Powell, A. K.; Heath, S. L. *J. Chem. Soc., Dalton Trans.* **2000**, 1835−1840. (g) Christou, G.; Gatteschi, D.; Hendrickson, D. N.; Sessoli, R. *MRS Bull.* **2000**, *25*, 66−71. (h) Tsai, H.-L.; Jwo, T.-Y.; Lee, G.-H.; Wang, Y. *Chem. Lett.* **2000**, 346−347. (i) Aubin, S. M. J.; Sun, Z.; Eppley, H. J.; Rumberger, E. M.; Guzei, I. A.; Folting, K.; Gantzel, P. K.; Rheingold, A. L.; Christou, G.; Hendrickson, D. N. *Inorg. Chem.* **2001**, *40*, 2127−2146. (j) Park, C.-D.; Rhee, W.; Kim, Y.; Jeon, W.; Jung, D.-Y.; Kim, D.; Do, Y.; Ri, H.-C. *Bull. Korean Chem. Soc.* **2001**, *22*, 453−454. (k) Kuroda-Sowa, T.; Lam, M.; Rheingold, A. L.; Frommen, C.; Reiff, W. M.; Nakano, M.; Yoo, J.; Maniero, A. L.; Brunel, L.-C.; Christou, G.; Hendrickson, D. N.; *Inorg. Chem.* **2001**, *40*, 6469−6480. (l) Kuroda-Sowa, T.; Fukuda, T.; Miyoshi, S.; Maekawa, M.; Munakata, M.; Miyasaka, H.; Yamashita, M. *Chem. Lett.* **2002**, *7*, 682−683.

(3) (a) Aubin, S. M. J.; Wemple, M. W.; Adams, D. M.; Tsai, H.-L.; Christou, G.; Hendrickson, D. N. *J. Am. Chem. Soc.* **1996**, *118*, 7746−7754. (b) Aubin, S. M. J.; Dilley, N. R.; Pardi, L.; Krzystek, J.; Wemple, M. W.; Brunel, L.-C.; Maple, M. B.; Christou, G.; Hendrickson, D. N. *J. Am. Chem. Soc.* **1998**, *120*, 4991−5004. (c) Andres, H.; Basler, R.; Güdel, H.-U.; Aromí, G.; Christou, G.; Büttner, H.; Rufflé, B. *J. Am. Chem. Soc.* **2000**, *122*, 12469−12477.

(4) (a) Brechin, E. K.; Yoo, J.; Nakano, M.; Huffman, J. C.; Hendrickson, D. N.; Christou, G. *Chem. Commun.* **1999**, 783−784. (b) Yoo, J.; Brechin, E. K.; Yamaguchi, A.; Nakano, M.; Huffman, J. C.; Maniero, A. L.; Brunel, L.-C.; Awaga, K.; Ishimoto, H.; Christou, G.; Hendrickson, D. N. *Inorg. Chem.* **2000**, *39*, 3615−3623.

(5) Yoo, J.; Yamaguchi, A.; Nakano, M.; Krzystek, J.; Streib, W. E.; Brunel, L.-C.; Ishimoto, H.; Christou, G.; Hendrickson, D. N. *Inorg. Chem.* **2001**, *40*, 4604−4616.

(6) Barra, A. L.; Caneschi, A.; Cornia, A.; Fabrizi de Biani, F.; Gatteschi, D.; Sangregorio, C.; Sessoli, R.; Sorace, L. *J. Am. Chem. Soc.* **1999**, *121*, 5302−5310.

(7) Oshio, H.; Hoshino, N.; Ito, T. *J. Am. Chem. Soc.* **2000**, *122*, 12602−12603.

(8) Castro, S. L.; Sun, Z.; Grant, C. M.; Bollinger, J. C.; Hendrickson, D. N.; Christou, G. *J. Am. Chem. Soc.* **1998**, *120*, 2365−2375.

(9) Clérac, R.; Miyasaka, H.; Yamashita, M.; Coulon, C. *J. Am. Chem. Soc.* **2002**, *124*, 12837−12844.

(10) Caneschi, A.; Gatteschi, D.; Lalioti, N.; Sangregorio, C.; Sessoli, R.; Venturi, G.; Vindigni, A.; Rettori, A.; Pini, M. G.; Novak, M. A. *Angew. Chem., Int. Ed.* **2001**, *40*, 1760−1763. Caneschi, A.; Gatteschi, D.; Lalioti, N.; Sessoli, R.; Sorace, L.; Tangoulis, V.; Vindigni, A. *Chem. Eur. J.* **2002**, *8*, 286−292. Caneschi, A.; Gatteschi, D.; Lalioti, N.; Sangregorio, C.; Sessoli, R.; Venturi, G.; Vindigni, A.; Rettori, A.; Pini, M. G.; Novak, M. A. *Europhys. Lett.* **2002**, *58*, 771−777. Lescouëzec, R.; Vaissermann, J.; Ruiz-Pérez, C.; Lloret, F.; Carrasco, R.; Julve, M.; Verdaguer, M.; Dromzee, Y.; Gatteschi, D.; Wernsdorfer, W. *Angew. Chem., Int. Ed.* **2003**, *42*, 1483−1486. Toma, L. M.; Lescouëzec, R.; Lloret, F.; Julve, M.; Vaissermann, J.; Verdaguer, M. *Chem. Commun.* **2003**, 1850−1851.

(11) Glauber, R. J. *J. Math. Phys.* **1963**, *4*, 294−307.

(12) (a) Suzuki, M.; Kubo, R *J. Phys. Soc. Jpn.* **1968**, *24*, 51−60. (b) Stanley, R *Phase Transition and Critical Phenomena*; Clarendon Press: Oxford, 1971; Appendix E, p 280.

Chart 1

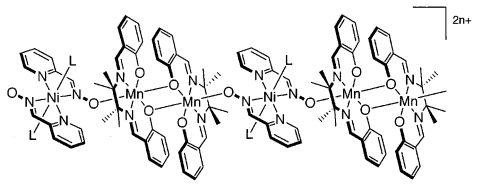

Type A: $[Mn_2(saltmen)_2Ni(pao)_2(L)_2](ClO_4)_2$

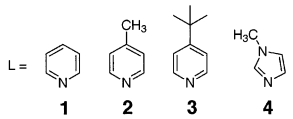

1 **2** **3** **4**

Type B: $[Mn_2(saltmen)_2Ni(pao)_2(py)_2](A)_2$
(py = pyridine; A = BF_4^-, **5**; PF_6^-, **6**; ReO_4^-, **7**)

chain. The study of its magnetic behavior demonstrates that the slow relaxation of the magnetization at low temperatures is induced by the strong anisotropic Co^{II} metal ion and a strong Co^{II}−radical magnetic interaction. Nevertheless, the helical arrangement of the cobalt local anisotropy tensors leads to a complex magnetic behavior superposed to the slow relaxation process. More recently, we have reported a new SCM compound, $[Mn_2(saltmen)_2Ni(pao)_2(py)_2](ClO_4)_2$ (**1**) (saltmen^{2-} = *N*,*N*′-(1,1,2,2-tetramethylethylene) bis(salicylideneiminate), pao$^-$ = pyridine-2-aldoximate, py = pyridine).[9] Compound **1** consists of two fragments, an out-of-plane Mn^{III} dimer, $[Mn_2(saltmen)_2]^{2+}$, and a neutral mononuclear Ni^{II} unit, $Ni(pao)_2(py)_2$, forming an alternating linear chain having ferromagnetically coupled $S = 3$ repeating units, [−Mn−ON−Ni−NO−Mn−$(O)_2$−]. Each chain is structurally and magnetically well isolated by the counteranions and bulky ligands. As expected, combined ac and dc magnetic measurements revealed slow relaxation of the magnetization, i.e., single-chain magnet behavior. It is worth noticing that this material has an easy axis parallel to the unique chain orientation[9] and can therefore be a model system to study the dynamics of SCMs. Another appealing point of this compound is the possibility of easily chemically modifying its structural components such as the unidentate ligand (L) on the Ni^{II} metal ion (for **1**, L = pyridine) or the counteranion (for **1**, A = ClO_4^-). On the basis of this idea, we have oriented our research to design a series of closely related compounds to confirm the immutable character of the SCM behavior observed in **1**.

Therefore, we herein report on the first series of single-chain magnets $[Mn_2(saltmen)_2Ni(pao)_2(L)_2](A)_2$ (L = unidentate neutral ligand, A$^-$ = counteranion) (Chart 1). For this purpose, we prepared the following new building blocks: $Ni(pao)_2(L)_2$ (L = 4-picoline, 4-*tert*-butylpyridine, *N*-methylimidazole),[13] $[Mn_2(saltmen)_2(H_2O)_2](A)_2$ (A = ClO_4^-, BF_4^-, PF_6^-), and $Mn_2(saltmen)_2(ReO_4)_2$. The use of these precursors leads to a new family of heterometallic Mn^{III}−Ni^{II} chains (see Chart 1): $[Mn_2(saltmen)_2Ni(pao)_2(L)_2](ClO_4)_2$ where L = 4-picoline; **2**, 4-*tert*-butylpyridine; **3**, *N*-methylimidazole; **4**, and $[Mn_2(saltmen)_2Ni(pao)_2(py)_2](A)_2$ where A = BF_4^-; **5**, PF_6^-; **6**, ReO_4^-; **7**. The synthesis, structural characterization, and magnetic properties of these compounds will be discussed in relation with SCM behavior observed in **1**.

Results and Discussion

Syntheses. In order to investigate the influence of the chain environment on the magnetic properties, particularly on the SCM behavior, we have synthesized a series of $[Mn_2(saltmen)_2Ni(pao)_2(py)_2](ClO_4)_2$ derivatives. Here, two types of strategy have been used to modulate the neighborhood of the chains: (i) We have substituted pyridine ligands on the Ni^{II} metal ion of **1** by more bulky ligands and obtained the family of compounds $[Mn_2(saltmen)_2Ni(pao)_2(L)_2](ClO_4)_2$ (L = 4-picoline; **2**, 4-*tert*-butylpyridine; **3**, *N*-methylimidazole; **4**). To synthesize these compounds, coordination-donor building blocks of $Ni(pao)_2(L)_2$ (L = 4-picoline, 4-*tert*-butylpyridine, *N*-methylimidazole) were newly synthesized[13] and reacted with a coordination-acceptor building block, $[Mn_2(saltmen)_2(H_2O)_2](ClO_4)_2$. (ii) We also managed to exchange ClO_4^- anions with new counteranions by using $[Mn_2(saltmen)_2(H_2O)_2](A)_2$ (A = BF_4^-, PF_6^-) and $Mn_2(saltmen)_2(ReO_4)_2$ building blocks in reactions with $Ni(pao)_2(py)_2$: $[Mn_2(saltmen)_2Ni(pao)_2(py)_2](A)_2$ (A = BF_4^-; **5**, PF_6^-; **6**, ReO_4^-; **7**) (Chart 1). The $[Mn_2(saltmen)_2Ni(pao)_2(L)_2](A)_2$ series was thus synthesized in a methanol/water medium by the direct reaction of adequate building blocks in a molar ratio of 1:2, i.e., 1 equiv of Mn dimer for 2 equiv of Ni building block (indeed, a Mn/Ni = 1:1 ratio). It is noteworthy that this assembly reaction leads to a Mn/Ni = 2:1 stoichiometry compound in high yield, which was not improved by changing the Mn/Ni reaction ratio as observed in the assembly of **1**. Although an equilibrium between the monomeric $[Mn(saltmen)]^+$ and dimeric $[Mn_2(saltmen)_2]^{2+}$ species generally occurs in methanol/water media,[14b] this result indicates that the $Ni(pao)_2(L)_2$ monomer reacts selectively with the $[Mn_2(saltmen)_2]^{2+}$ dimer in this reaction condition. The origin of this selectivity has not been clearly identified, but it could be due to a coordination affinity of the Ni^{II} donor building blocks regardless of attaching ligands, L, and also due to packing effects of the final materials. Further studies are currently conducted to elucidate the mechanism of this selectivity. From these reactions, dark brown microcrystals of all compounds have been obtained within 2−3 days. Except for **3** which forms very small needle-shaped crystals, other syntheses lead to rectangular-shaped crystals which grow together to form complicated crops after 3 days of crystallization.

X-ray Diffraction Analysis. Single crystals of **4**, **6**, and **7** suitable for single-crystal X-ray crystallography have been

(13) Miyasaka, H.; Mizushima, K.; Sugiura, K.; Yamashita, M. *Synth. Met.* **2003**, *137*, 1245−1246.

(14) (a) The core geometry of the out-of-plane dimeric fragment is similar to what is found in the starting material $[Mn_2(saltmen)_2(H_2O)_2](ClO_4)_2$ ($Mn-O_{bridge}$ = 2.434(2) Å, Mn−O−Mn = 101.58(10)°, O_{bridge}−Mn−O_{bridge} = 78.42(10)°, Mn···Mn = 3.381(1) Å). (b) Miyasaka, H.; Clérac, R.; Ishii, T.; Chang, H.; Kitagawa, S.; Yamashita, M. *J. Chem. Soc., Dalton Trans.* **2002**, 1528−1534. Miyasaka, H.; Mizushima, K.; Furukawa, S.; Sugiura, K.; Ishii, T.; Yamashita, M. *Mol. Cryst. Liq. Cryst.* **2002**, *379*, 171−178. Miyasaka, H.; Sugimoto, K.; Sugiura, K.; Ishii, T.; Yamashita, M. *Mol. Cryst. Liq. Cryst.* **2002**, *379*, 197−204.

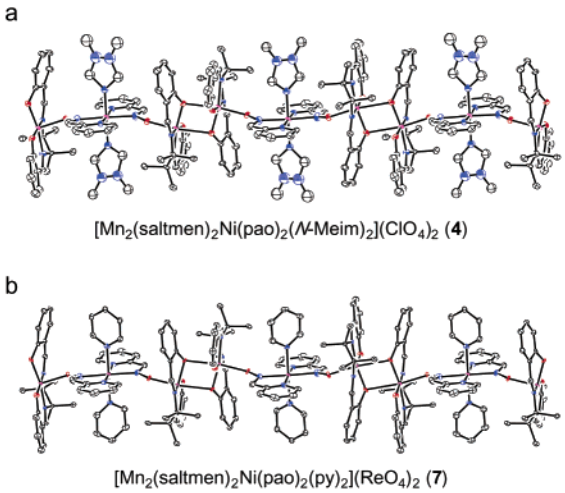

Figure 1. ORTEP views of the one-dimensional structures (a) for $[Mn_2(saltmen)_2Ni(pao)_2(N\text{-}Meim)_2](ClO_4)_2$ (**4**) and (b) for $[Mn_2(saltmen)_2Ni(pao)_2(py)_2](ReO_4)_2$ (**7**) (a similar view can be obtained for $[Mn_2(saltmen)_2Ni(pao)_2(py)_2](PF_6)_2$ (**6**)).

obtained as described in the previous part. Compounds **4**, **6**, and **7** crystallized in the same monoclinic space group, *C*2/*c* (No. 15), and are isostructural to **1**. These compounds are constituted of separated one-dimensional chains and counteranions, without crystallization solvent. Figure 1 shows ORTEP drawings of one-dimensional motifs for **4** and **7**, in which the oximato groups of $Ni^{II}(pao)_2(L)_2$ monomeric species bridge Mn^{III} saltmen dimers to form an alternating one-dimensional chain with a repeating unit of $[-(O_{ph})_2-Mn-ON-Ni-NO-Mn-]$.

Systematically, the 2-fold axis parallel to the *b* axis runs through the $Ni(pao)_2(L)_2$ moiety along the N(5)−Ni(1)−N(7) direction for **4**, or the N(5)−Ni(1)−N(6) direction for **6** and **7**. The coordination sphere of the Ni^{II} metal ion is a slightly distorted octahedron. Two pyridyloximate bidentate ligands (pao^-) occupy the in-plane positions around Ni(1) when two unidentate ligands, *N*-methylimidazole for **4** or pyridine for **6** and **7**, complete the coordination sphere in the axial positions as *trans* coordination mode (see Table 1 for bond distances and angles). It is important to note that the *trans* coordination geometry around Ni ion in the precursors, $Ni(pao)_2(L)_2$, is preserved in the final compound to built the one-dimensional assembly.[13] The oximato groups of $Ni(pao)_2(L)_2$ moieties bridge to Mn^{III} ion of $[Mn_2(saltmen)_2]^{2+}$ dimers to form the chain motif. In the term of bond distances and angles, this NO linkage between Mn^{III} and Ni^{II} ions is almost identical for all the structurally characterized compounds (see Table 1). This structural feature strongly suggests a similar magnetic interaction between Mn^{III} and Ni^{II} metal ions along the series (vide infra). The out-of-plane dimer, $[Mn_2(saltmen)_2]$, lies on an inversion center, and therefore, the asymmetric unit contains only one Mn^{III} moiety which assumes a square bipyramidal six-coordination geometry, where the equatorial coordination sites are occupied by the set of N(1), N(2), O(1), O(2) donor atoms of $saltmen^{2-}$ quadridentate ligand (equatorial average bond distances are $\langle Mn-N\rangle = 1.989$ Å and $\langle Mn-O\rangle = 1.893$ Å). Much longer bond distances (see Table 1) are found in the axial position occupied by the phenolate oxygen O(1*) arising from the

Table 1. Relevant Bond Distances (Å) and Angles (deg) around the Coordinated Metal Ions for **1**, **4**, **6**, and **7** with the Estimated Standard Deviations in Parentheses

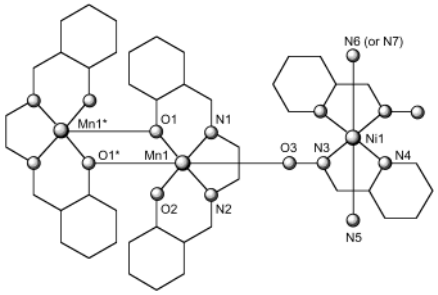

	1	4	6	7
	Bonds [Å]			
Ni1−N3	2.063(4)	2.058(8)	2.081(4)	2.070(7)
Ni1−N4	2.106(4)	2.100(7)	2.104(4)	2.099(7)
Ni1−N5	2.149(5)	2.005(8)	2.119(5)	2.12(1)
Ni1−N6 (or N7)[a]	2.150(5)	2.044(8)	2.126(5)	2.134(9)
Mn1−O1	1.910(3)	1.907(5)	1.903(3)	1.914(6)
Mn1−O2	1.870(3)	1.878(5)	1.876(3)	1.883(6)
Mn1−O3	2.116(3)	2.106(5)	2.100(3)	2.122(5)
Mn1−O1*[b]	2.551(3)	2.503(6)	2.537(3)	2.470(5)
Mn1−N1	1.988(3)	1.992(6)	1.993(3)	1.996(7)
Mn1−N2	1.981(3)	1.992(7)	1.981(3)	1.988(6)
	Angles [deg]			
N3−Ni1−N4	77.8(2)	77.9(3)	77.54(18)	77.6(3)
N3−Ni1−N5	90.8(1)	91.4(2)	90.76(13)	90.9(2)
N4−Ni1−N5	88.0(1)	88.3(2)	88.7(1)	87.9(2)
N3−Ni1−N6 (or N7)[a]	89.2(1)	88.6(2)	89.24(13)	89.1(2)
N4−Ni1−N6 (or N7)[a]	92.0(1)	91.7(2)	91.3(1)	92.1(2)
N5−Ni1−N6 (or N7)[a]	180	180	180	180
O1−Mn1−O1*[b]	81.1(1)	80.7(1)	80.5(1)	81.2(2)
O1−Mn1−O2	93.3(1)	93.7(2)	93.41(12)	93.7(2)
O1−Mn1−O3	90.9(1)	91.1(2)	91.66(11)	90.8(2)
O2−Mn1−O3	98.4(1)	98.2(2)	97.58(12)	96.7(2)
O1−Mn1−N1	91.3(1)	91.1(2)	91.47(13)	91.2(3)
O2−Mn1−N1	173.0(1)	173.2(3)	173.06(14)	173.8(3)
O3−Mn1−N1	86.8(1)	86.6(2)	87.20(13)	87.1(2)
O1−Mn1−N2	166.1(1)	166.2(3)	165.67(12)	167.0(2)
O2−Mn1−N2	92.9(1)	92.8(2)	92.80(13)	92.3(3)
O3−Mn1−N2	100.5(1)	100.0(3)	100.30(12)	99.9(2)
N1−Mn1−N2	81.5(1)	81.5(3)	81.35(14)	82.2(3)
Ni1−N3−O3	123.9(3)	125.8(6)	127.0(3)	124.7(5)
Mn1−O3−N3	131.8(2)	134.9(5)	132.4(3)	133.4(5)
Mn1−O1−Mn1*[b]	98.9(1)	99.3(2)	99.5(1)	98.8(2)

[a] N7 in **4**. [b] Symmetry operation (*): $^1/_2 - x$, $^1/_2 - y$, $-z$.

neighboring $[Mn(saltmen)]^+$ moiety forming the out-of-plane dimer [Mn−O(1*) = 2.470(5)−2.537(3) Å] and the oximato oxygen O(3) arising from the $Ni(pao)_2(py)_2$ moiety [Mn−O(3) = 2.100(3)−2.122(5) Å].[14] This elongated axis is well-known to be the signature of a Jahn−Teller distortion in Mn^{III} complexes as observed in the precursor, $[Mn_2(saltmen)_2(H_2O)_2](ClO_4)_2$, and its derivatives.[14b]

As an illustration of the general packing diagram of this series, Figure 2 shows two projection views of **6**. Each chain runs in the *ac* plane along the $(a + c)$ direction (Figure 2a) and is separated from the nearest chains with a minimum intermetallic distance between Mn and Ni ions of 10.36 Å for **4**, 10.51 Å for **6**, and 10.30 Å for **7** (10.39 Å for **1**). As shown in Figure 2b, counteranions are evenly located between chains. Thus, the arrangement of these counteranions could play an important role in isolating the chains. Although the size of ReO_4^- is much bigger than ClO_4^- or PF_6^- counteranions, M···M interchain distances are not increasing

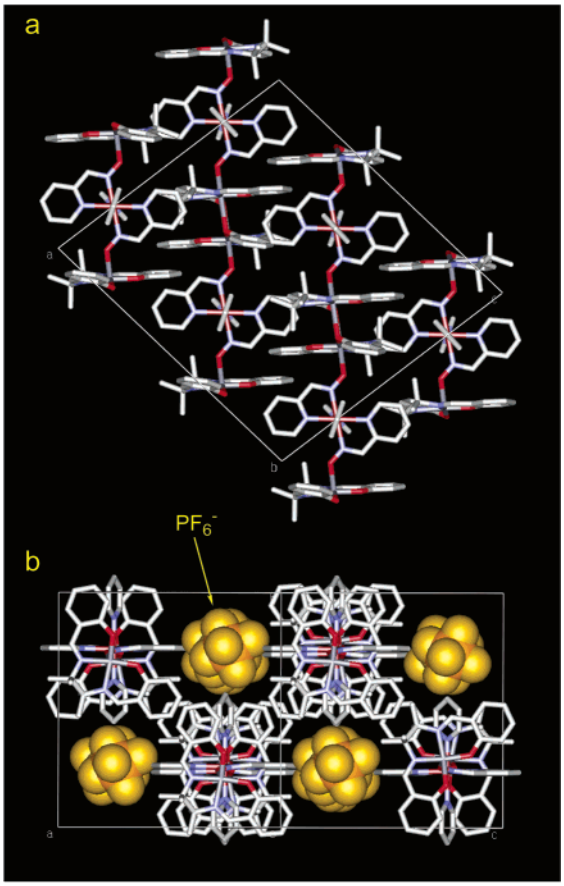

Figure 2. Packing diagram of **6** showing (a) the projection in the *ac* plane where the chains are running in the (*a*+*c*) direction (PF_6^- counterions located between chains and hydrogen atoms are omitted for clarity) and (b) the projection along the chain axis.

with the size of the anions. On the contrary, the shortest and longest M···M interchain distances are found for the materials containing the biggest (ReO_4^-, **7**) and smallest (PF_6^-, **6**) counteranions, respectively. It clearly suggests that the chains are mainly responsible for the packing of the crystal structure, and in fact, the counteranions only fill up the remaining void space. Therefore, the three-dimensional arrangement of the chains is essentially the same for all compounds including **1**. At this point, it is also important to note for the magnetic discussion (vide infra) that no significant interchain weak interactions, like interchain $\pi-\pi$ stacking between phenyl rings coming from the saltmen ligands, are observed in **1**, **4**, **6**, and **7**.

X-ray diffraction analyses on powder samples have been performed to further investigate the structural characteristics of these compounds. As shown Figure 3, **1**, **2**, and **4**−**7** exhibit nearly identical powder patterns: these six compounds are certainly crystalline and isostructural. As expected, simulation of powder patterns (red lines in Figure 3) predicted from single-crystal structures of **1**, **4**, **6**, and **7** are in excellent agreement with the experimental data. On the basis of the indexation of the (0,2,0) and (−2,0,2) diffraction peaks, only small changes on the interchain distances are observed among the series. Representatively, the (0,2,0) and (2,0,2) diffraction peaks slightly shifted among the series within a range −0.3° to +0.04° compared

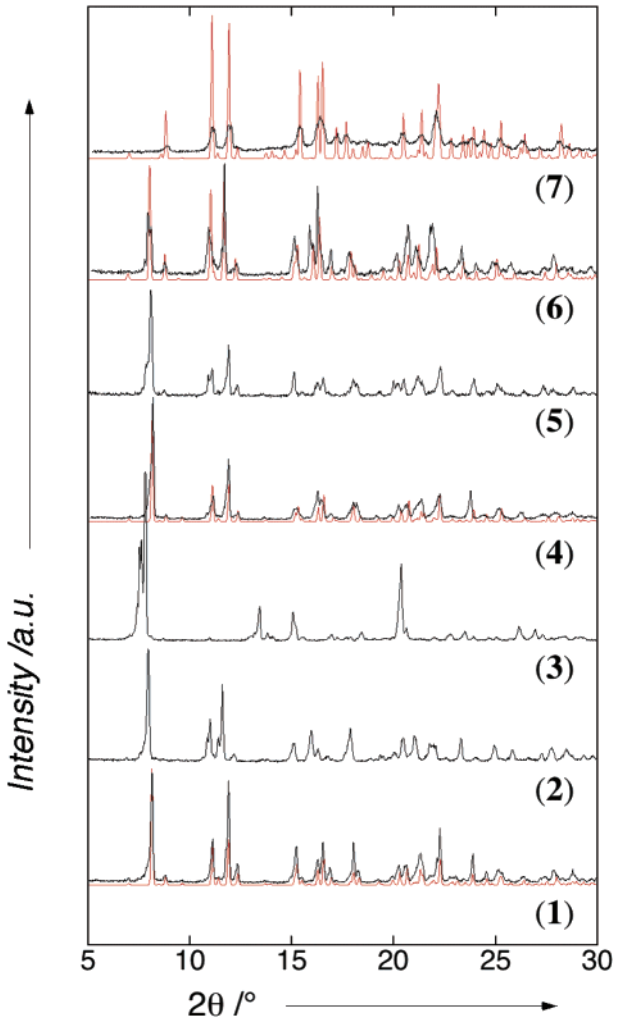

Figure 3. X-ray powder diffraction patterns for the whole series of $[Mn_2(saltmen)_2Ni(pao)_2(L)_2](A)_2$. Red lines are the simulated X-ray powder diffraction patterns obtained from the single-crystal structural data.

to $2\theta = 11.07°$ and 11.86° observed in **1**, respectively. This implies that the packing is mainly controlled by the chain arrangement, which allows enough interchain space to accommodate the different chemical modifications (variation of counteranion and attached ligand). On the other hand, the powder X-ray diffraction of **3** reveals its crystalline nature but also a completely different pattern from the other compounds, indicating the presence of a peculiar crystal packing. It should be mentioned that compound **3** has, however, a similar one-dimensional motif to those of the other compounds, as shown by its magnetic properties mentioned hereafter.

Magnetic Properties. The dc magnetic measurements were performed on polycrystalline samples of **1**−**7** between 300 and 1.9 K under an external field of 1 kOe. For all compounds, the temperature dependence of $1/\chi$ (where χ is M/H) between 300 and 120 K obeys Curie−Weiss law roughly with $C = 6.7$ emu·K·mol^{-1} and $\theta = -28$ K for **2** (Figure 4), $C = 6.8$ emu·K·mol^{-1} and $\theta = -35$ K for **3**, $C = 6.7$ emu·K·mol^{-1} and $\theta = -26$ K for **4**, $C = 6.9$ emu·K·mol^{-1} and $\theta = -30$ K for **5**, $C = 6.7$ emu·K·mol^{-1} and $\theta = -25$ K for **6**, and $C = 6.8$ emu·K·mol^{-1} and $\theta =$

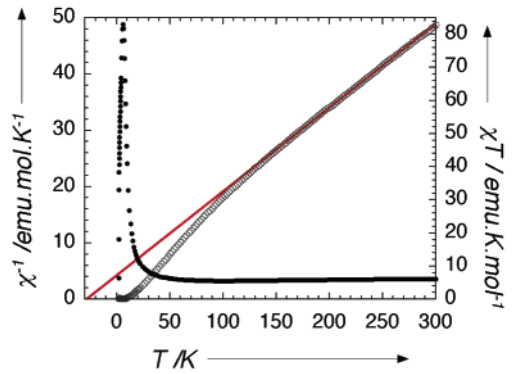

Figure 4. Temperature dependence of the inverse of the susceptibility (χ, ○) and the χT product (●) at 1000 Oe, measured on a polycrystalline sample of **2**. Red line corresponds to the best fit obtained with a Curie−Weiss law in the temperature range from 130 to 300 K.

−25 K for **7**. Obtained Curie constants are in good agreement with the expected spin only value, i.e., 7 emu·K·mol^{-1}, for two Mn^{III} ($S = 2$) and one Ni^{II} ($S = 1$) assuming an average g value of 2.0. The slightly lower value of C could be explained by an average g value of 1.96−1.99, taking into account that the same trend has been reported in **1** ($C = 6.8$ emu·K·mol^{-1}, $\theta = -26$ K, and $g = 1.97$). The negative sign of the Weiss constants indicates that the dominant interaction between spin carriers is antiferromagnetic,[15] as already observed in **1**. On the basis of the crystal structure analysis and a similarity to **1**, three possible pathways for magnetic interaction have been considered: the $Ni^{II}\cdots Mn^{III}$ interaction (J) via oximate bridge, the intrachain $Mn^{III}\cdots Mn^{III}$ interaction (J') in the out-of-plane dimer, and the weak interchain (J'') interactions. Magnetic interactions between Mn^{III} sites are expected to be weakly ferromagnetic as observed in related compounds having similar out-of-plane dimer forms.[14,16] Considering that the interchain interactions are weak, the Weiss constant reflects principally the $Ni^{II}\cdots Mn^{III}$ interaction (J) via the oximate bridge. Figure 4 shows the temperature dependence of χT for **2** as typical data among the series. With decreasing temperature, the χT product decreases gradually and shows a minimum around 100 K. Below this temperature, χT increases abruptly to reach a maximum around 6 K ($\chi T_{max} = 80-100$ cm^3·K·mol^{-1} at 6−7 K depending on the compounds), and finally decreases again at lower temperatures. The decrease of χT above 100 K is well understood by the antiferromagnetic contribution between Mn^{III} ions and Ni^{II} ions via oximate bridging as already considered in the Curie−Weiss behavior analysis (vide supra). However, the magnetic behavior below 100 K reveals the presence of weak ferromagnetic interaction as expected between Mn^{III} ions via phenolate bridging in the out-of-plane dimer (J').[9,14,16] It is worth noticing at this point that the observation of ferromagnetic exchange indicates that the ferromagnetic $Mn^{III}-Mn^{III}$ interaction (J') clearly overcomes the interchain antiferromagnetic ones (J'').[17] Therefore, the material looks like an assembly of trimers [Mn···Ni···Mn] with relatively strong $Ni^{II}\cdots Mn^{III}$ antiferromagnetic interactions (J) connected through weak ferromagnetic interactions (J').

As a first approach, the magnetic susceptibility of this system can be modeled by a simple $Mn^{III}-Ni^{II}-Mn^{III}$ trimer model ($S_{Mn} = 2$, $S_{Ni} = 1$), on the basis of the following Heisenberg Hamiltonian:

$$H = -2J(\mathbf{S}_{Mn1}\cdot\mathbf{S}_{Ni} + \mathbf{S}_{Ni}\cdot\mathbf{S}_{Mn2}) + g\mu_B S_{Tz} H_z \qquad (1)$$

where $\mathbf{S}_T$ refers to the total spin operator of the trimer as $\mathbf{S}_T = \mathbf{S}_{Mn1} + \mathbf{S}_{Ni} + \mathbf{S}_{Mn2}$ and S_{Tz} is the projection of $\mathbf{S}_T$ along the magnetic field applied in the z direction, H_z. Nevertheless, ferromagnetic intertrimer magnetic couplings (J') along the chain need to be considered to reproduce the χT increase below 100 K. As already mentioned, these interactions are significantly weaker than the intratrimer $Ni^{II}-Mn^{III}$ coupling. Therefore, this magnetic coupling has been treated in a mean field approximation

$$\chi = \frac{\chi_{trimer}}{1 - \frac{4J_i}{Ng^2\mu_B{}^2}\chi_{trimer}} \qquad (2)$$

where J_i is the sum of the magnetic interactions around each trimer which is surrounded by two trimers within a chain and by eight trimers on neighboring chains (see Figure 2), therefore $J_i = J' + 4J''$.

This model reproduces, with good agreement, the experimental data of all compounds above 30 K. The best sets of parameters obtained for **2**−**7** are summarized in Table 2, and as a representative example, the fitting of the data for **2** is shown in Figure 5. It should be mentioned that the calculated parameters are physically acceptable among the series and also in good agreement with the previous Curie−Weiss analysis. As expected from the structural description of **1**, **4**, **6**, and **7** (see Table 1 and Table 2), magnetic parameters are very similar, and no clear correlation with structural distances and angles has been observed. For the whole series, this result tends to prove that all compounds have a closely related one-dimensional structure although **3** exhibits a different X-ray powder pattern. The chain motif seems to be also preserved in **3** as suggested by magnetic data which fit well to the proposed model. Nevertheless, the peculiar nature of **3** can be seen in the magnetic exchange parameters of both J and J_i. The Ni···Mn antiferromagnetic interaction (J) seems to be slightly stronger than for others ($J/k_B = -24.2(2)$ K), and moreover, the magnetic interaction between trimers (J_i) is, on the contrary, slightly smaller ($J_i/k_B = +0.62(2)$ K). However, these deviations do not allow us to conclude if J_i is smaller due to a modification in the geometry of the out-of-plan dimer (with a decrease of J') or an enhancement of the interchain antiferromagnetic interaction, J''.

(15) The zero field splitting term is usually negligible for Mn^{III} and Ni^{II} systems ($|D| < 3$ K) compared to the magnetic interactions in this system and would only weakly affect a Weiss constant < -25 K.

(16) Sato, Y.; Miyasaka, H.; Matsumoto, N.; Okawa, H. *Inorg. Chim. Acta* **1996**, *247*, 57−63. Shyu, H.-L.; Wei, H.-H.; Wang, Y. *Inorg. Chim. Acta* **1999**, *290*, 8−13.

(17) Interchain magnetic interactions (J''), probably mediated by weak π overlaps of aromatic rings, are most likely antiferromagnetic.

Table 2. Important Structural Distances and Magnetic Parameters for **1**−**7**

compd	Mn−$O_{oximate}$ distance [Å]	Mn−O−N angle [deg]	Mn−$O_{phenolate}$ distance [Å]	Mn−O−Mn* angle [deg]	nearest interchain M−M distance [Å]	magnetic interaction[a] J/k_B[b] [K]	magnetic interaction[a] J_i/k_B[c] [K]	Arrhenius parameter τ_0 [s]	Arrhenius parameter Δ/k_B [K]
1[9]	2.116(3)	131.8(2)	2.551(3)	98.9(1)	10.39	−20.8(2)	+0.70(2)	$0.6(1) \times 10^{-10}$	72.0(2)
2						−22.2(2)	+0.71(2)	$0.8(1) \times 10^{-10}$	68.0(2)
3						−24.2(2)	+0.62(2)	$1.3(1) \times 10^{-10}$	68.3(2)
4	2.106(5)	134.9(5)	2.503(6)	99.3(2)	10.36	−22.2(2)	+0.76(2)	$1.0(1) \times 10^{-10}$	70.9(2)
5						−21.4(2)	+0.79(2)	$1.2(1) \times 10^{-10}$	67.6(2)
6	2.100(3)	132.4(3)	2.537(3)	99.5(1)	10.51	−21.5(2)	+0.80(2)	$1.2(1) \times 10^{-10}$	67.8(2)
7	2.122(5)	133.4(5)	2.470(5)	98.8(2)	10.30	−21.2(2)	+0.84(2)	$0.8(1) \times 10^{-10}$	72.6(2)

[a] The parameters obtained by best-fitting simulation using the Heisenberg trimer model of [$Mn^{III}\cdots Ni^{II}\cdots Mn^{III}$] ($S = 2, 1, 2$) with intertrimer interactions treated in a mean-field approximation in the temperature range 30−300 K (see text); note that the average g value was fixed at 1.99. [b] The J/k_B refers to the intratrimer magnetic interaction between Mn^{III} and Ni^{II} ions via oximate bridge. [c] The J_i/k_B refers to the intertrimer magnetic exchange interaction.

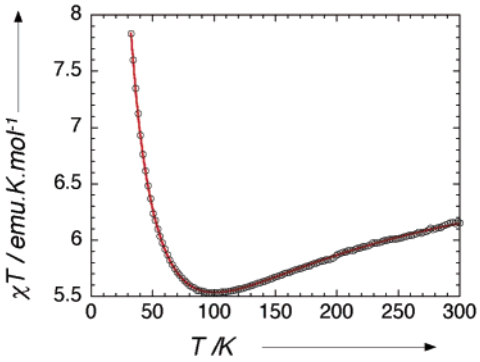

Figure 5. Temperature dependence of the χT product above 30 K, measured at 1000 Oe on a polycrystalline sample of **2**. Red line corresponds to the best fit simulated with a model of [$Mn^{III}\cdots Ni^{II}\cdots Mn^{III}$] trimer including intertrimer interactions via mean field approximation (see text).

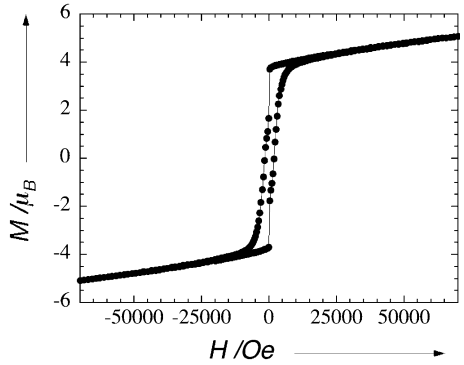

Figure 6. Field dependence of the magnetization on a powder sample of **2** at 1.8 K with a field sweep rate of about 20 Oe/s. Solid line is guide for eyes. Coercive fields at 1.9 K with a field sweet rate of about 20 Oe/s are 2500, 1300, 1100, 300, 900, 600, and 2500 Oe on polycrystalline samples of **1**, **2**, **3**, **4**, **5**, **6**, and **7**, respectively.

For the whole series, field dependence of the magnetization below 3.5 K reveals the presence of hysteresis loops (e.g., for a polycrystalline sample of **2** in Figure 6) and indicates a magnet-type behavior. The observation of this bi-stability on polycrystalline samples confirms the characteristic behavior already reported on oriented single crystals of **1**.[9] Even at high fields, the magnetization is not saturated at the expected value of 6 μ_B. This result can be easily understood taking into account the polycrystalline nature of the sample and the strong magnetic anisotropy observed on single crystal on **1**.[9] Indeed, when measured in the easy direction (Figure 7), the magnetization on a single crystal of **1** reveals as expected a rapid saturation. As shown Figure 7b, the hysteresis loops are strongly field sweep rate dependent as

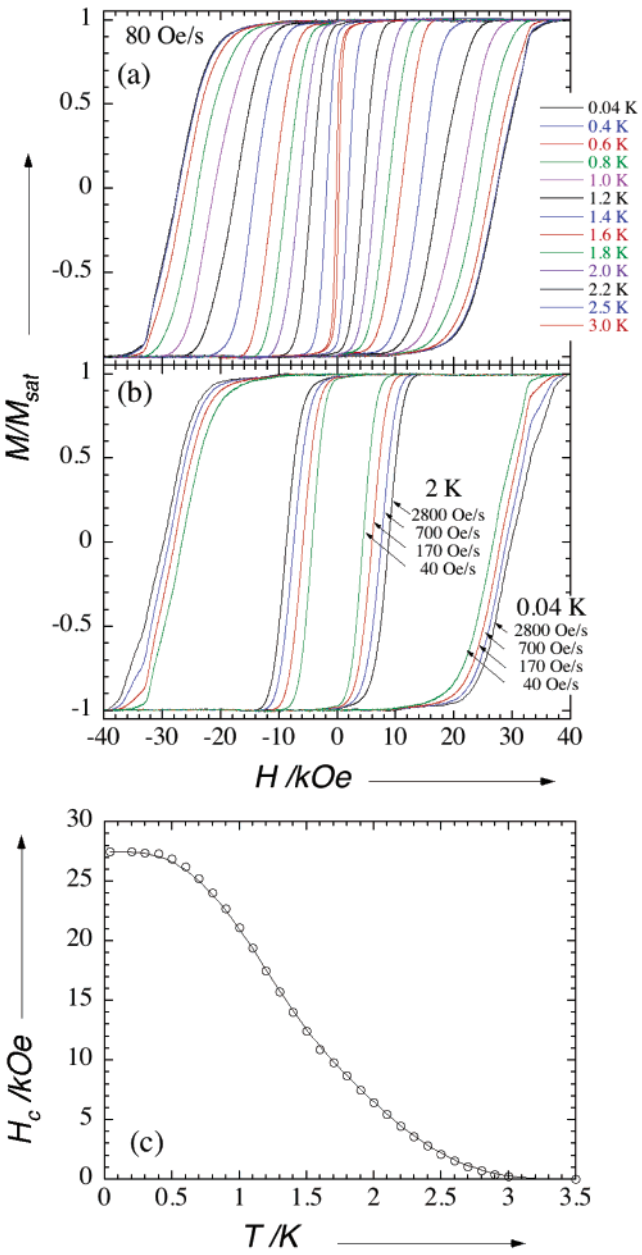

Figure 7. Measurements on a single crystal of **1** in the easy direction (chain axis). Field dependence of the magnetization (a) at different temperature with 80 Oe/s field sweep rate and (b) at 2 and 0.04 K at different field sweep rates. (c) Temperature dependence of the coercive field with 80 Oe/s field sweep rate.

expected for slow relaxing systems. The coercive field increases very rapidly with lowering temperature (Figure

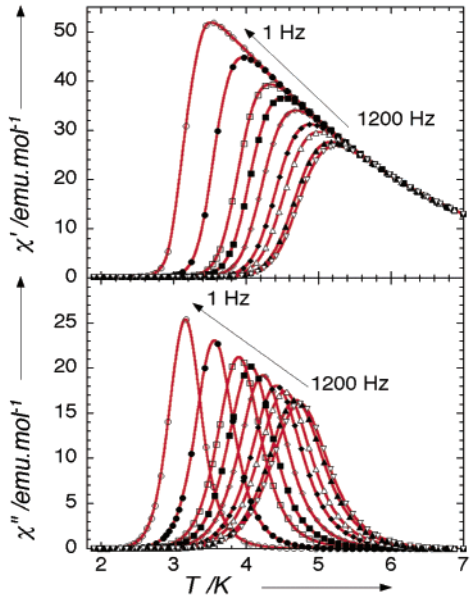

Figure 8. Temperature and frequency dependence of the real (χ') and imaginary (χ'') parts of the ac susceptibility for **2**. Red lines are only guide for eyes.

7a,c) to reach 27500 Oe at 0.4 K. Below this temperature, the coercive field becomes temperature independent at a given field sweep rate, but it is also important to note that the hysteresis remains strongly field sweep rate dependent even at 0.04 K (Figure 7b). This behavior is similar to SMM materials where the dynamics at very low temperature is dominated by quantum effects.[18] In order to get more insight into the observed magnetic behavior, ac magnetic measurements have been performed for **1**−**7**.

The frequency dependence of ac susceptibilities was measured in the temperature range 1.9−7 K under an oscillating magnetic field of 1 Oe or 3 Oe. Below 6.5 K, χ' and χ'', defined as the real and imaginary components of the ac susceptibility, respectively, are strongly frequency dependent in all compounds. It should be first mentioned that the overall feature of the frequency dependent behavior is very similar across the series indicating that the slight modification at the molecular level of the counteranions and attaching ligand seems to be of very weak influence on the ac magnetic behavior. Figure 8 shows the representative ac susceptibility features of **2** measured at various ac frequencies (1−1200 Hz). As concluded in the preliminary report for **1**,[9] this result unambiguously precludes any three-dimensional ordering but indicates the presence of slow relaxation of the magnetization as observed for SCM,[9,10,11] SMM,[1−8] superparamagnetic nanoparticles,[19] or spin-glass-like materials.[20] Below the blocking temperature, $T_B(\nu_{ac})$, the magnetization of these systems has not enough thermal energy to follow

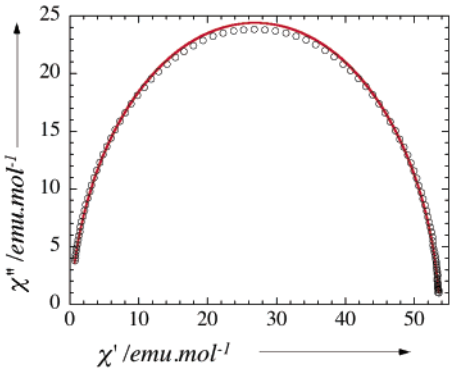

Figure 9. Cole−Cole diagram at 4.0 K for **2**. The solid red line represents the least-squares fit obtained with a generalized Debye model (see text) with $\alpha = 0.06$, $\chi_\infty = 53.6$ emu/mol, and χ_0 fixed at 0.

the applied oscillating field at a given frequency (ν_{ac}). Therefore, at this frequency, the entire magnetization becomes frozen below T_B, and the ac response vanishes in parallel to the appearance of coercivity. As expected, experimental data described in Figures 6−8 confirm the relevance of this scenario: the ac responses vanish when the coercivity appears. It seems clear that SMM or superparamagnetic nanoparticle behavior can be easily ruled out on the basis of the previous description of the materials (crystalline nature and also one-dimensional structure); nevertheless, even if unlikely,[21] the spin-glass interpretation cannot be directly abandoned. Therefore, a detailed study of the ac susceptibility needs to be performed. At a fixed temperature and without applied magnetic field, χ' and χ'' were measured as a function of the ac frequency, ν_{ac}, ranging from 1 to 1500 Hz. From these measurements, Cole−Cole diagrams (χ'' vs χ' plot) have been obtained for all compounds and exhibit systematically only one relaxation process proved by a nearly semicircle shape. A representative Cole−Cole plot at 4 K is depicted in Figure 9 for **2**. The ac susceptibility has been simulated using a generalized Debye model[22]

$$\chi'(\nu_{ac}) = \chi_\infty + \frac{(\chi_0 - \chi_\infty)[1 + (2\pi\nu_{ac}\tau)^{1-\alpha}\sin(\alpha\pi/2)]}{1 + 2(2\pi\nu_{ac}\tau)^{1-\alpha}\sin(\alpha\pi/2) + (2\pi\nu_{ac}\tau)^{2(1-\alpha)}} \quad (3)$$

$$\chi''(\nu_{ac}) = \frac{(\chi_0 - \chi_\infty)(2\pi\nu_{ac}\tau)^{1-\alpha}\cos(\alpha\pi/2)}{1 + 2(2\pi\nu_{ac}\tau)^{1-\alpha}\sin(\alpha\pi/2) + (2\pi\nu_{ac}\tau)^{2(1-\alpha)}} \quad (4)$$

where χ_∞ is the adiabatic susceptibility extrapolated when $\nu_{ac} \rightarrow \infty$, χ_0 is the isothermal susceptibility extrapolated when $\nu_{ac} \rightarrow 0$, and τ is the average relaxation time of magnetization. The α parameter, which ranges between 0 and 1, quantifies the width of the τ distribution.[22] When $\alpha = 0$,

(18) Wernsdorfer W.; Coulon, C.; Clérac, R.; Miyasaka, H. Manuscript in preparation.
(19) Morrish, A. H. *The Physical Principles of Magnetism*; Wiley: New York, 1965. Bean, C.; Livingston, J. D. *J. Appl. Phys.* **1959**, *30*, 120S−129S.
(20) Mydosh, J. A. *Spin Glasses: An Experimental Introduction*; Taylor & Francis: London, 1993. Chowdhury, D. *Spin Glasses and Other Frustrated Systems*; Princeton University Press: Princeton, NJ, 1986. Moorjani, K.; Coey, J. M. *Magnetic Glasses*; Elsevier: New York, 1984. Binder, K.; Young, A. P. *Rev. Mod. Phys.* **1986**, *58*, 801−976.
(21) The occurrence of a true spin-glass behavior is in fact very unlikely taking into account that this type of material needs to possess frustration at all energy levels. This is difficult to imagine in a one-dimensional system.
(22) Cole, K. S.; Cole, R. H. *J. Chem. Phys.* **1941**, *9*, 341. Boettcher, C. J. F. *Theory of electric polarisation*; Elsevier: Amsterdam, 1952. Aubin, S. M.; Sun, Z.; Pardi, L.; Krzysteck, J.; Folting, K.; Brunel, L.-J.; Rheingold, A. L.; Christou, G.; Hendrickson, D. N. *Inorg. Chem.* **1999**, *38*, 5329−5340.

eqs 3 and 4 are reduced to the Debye model involving a single relaxation time. Indeed, the experimental data are well reproduced by an ideal Debye model, and only the introduction of a small α value is necessary to perfectly fit the Cole−Cole diagrams: 0.05 for **1**, 0.06 for **2** (Figure 9), 0.05 for **3**, 0.15 for **4**, 0.11 for **5**, 0.12 for **6**, and 0.11 for **7**. Although the generalized Debye model has been used extensively to describe relaxation processes with a distribution of relaxation times,[22,23] the observation of small α values and symmetrical Cole−Cole plot shapes clearly indicates that the present relaxation process can be considered with a single relaxation time (excluding an interpretation as a spin-glass or random-domain magnet).

Taking into account that only one relaxation process occurs in these materials with a single relaxation time, the blocking temperature $T_B(\nu_{ac})$ can be deduced experimentally, from the maximum of the $\chi''(\nu)$ curve. At this temperature, the relaxation time of the system τ is equal to the characteristic time of the experience (τ_{exp}): $\tau(T_B) = \tau_{exp} = 1/(2\pi\nu_{ac})$. According to the Glauber's theory for one-dimensional Ising system,[11,12,24] the relaxation time follows an activated law

$$\tau(T) = \tau_i(T)\exp\left(\frac{8J'S_T^2}{k_BT}\right) \qquad (5)$$

where the pre-exponential factor τ_i introduced phenomenologically by R. J. Glauber describes the individual dynamics of the spin unit composing a chain, and therefore, generally depends on temperature.[12a,25] In the simple case of anisotropic isolated units (i.e., in the SMM case, $J' = 0$), we expect that τ_i follows an activated law

$$\tau_i(T) = \tau_0 \exp\left(\frac{|D|S_T^2}{k_BT}\right) \qquad (6)$$

where D is the single ion anisotropy (here $D < 0$ for uniaxial anisotropy)[26] and τ_0 is a pre-exponential factor characteristic of the system. An experimental illustration of this Arrhenius law (eq 6) is given by the relaxation of single-molecule magnets when the thermal activation is dominant over quantum tunneling.[27] In the case of the anisotropic units coupled ferromagnetically along a chain, the overall behavior is hence given by

$$\tau(T) = \tau_0 \exp\left(\frac{\Delta}{k_BT}\right) \qquad (7)$$

where $\Delta = (8J' + |D|)S_T^2$ is the energy barrier to reverse the magnetization direction (vide infra).[25] As shown in Figure 10, plots of $1/T_B$ versus $\ln(2\pi\nu_{ac})$ for the whole series of compounds follow a linear variation that confirms the theoretical predictions of eq 7.[28] Fitting to the Arrhenius equation leads to the pre-exponential factors (τ_0's) and characteristic energies (Δ's) summarized in Table 2. We should first comment that along with the crystalline nature of the materials and the lack of frustrated magnetic interactions, the obtained parameters τ_0 and Δ are physically meaningful and preclude a spin-glass interpretation of the magnetic data or a critical slowing down due to interchain interactions. Therefore, as already demonstrated for **1**, this family of materials exhibits a single-chain magnet behavior. The τ_0 and Δ/k_B obtained in the series are very similar, $\tau_0 \approx 1 \times 10^{-10}$ s and $\Delta/k_B \approx 70$ K, emphasizing the weak influence of the chemical modifications (counteranion, ligands) and interchain interactions on the magnetic properties of these compounds.

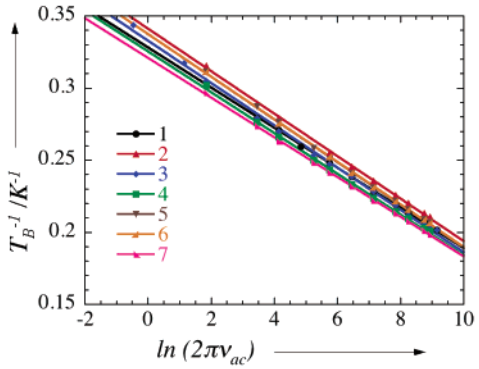

Figure 10. $1/T_B$ versus $\ln(2\pi\nu_{ac})$ plots. The solid lines represent the least-squares linear fits of the experimental data with the Arrhenius equation (see text).

As already mentioned, the energy gap Δ for a chain built with ferromagnetically coupled anisotropic units should be theoretically equal to $(8J' + |D|)S_T^2$.[25] To compare the values of Δ deduced from the Arrhenius plots (Figure 10 and Table 2), J' and D need to be determined. J' can be roughly identified to the J_i interaction[29] which was already evaluated by two techniques: from the mean-field model of the magnetic susceptibility above 30 K (vide supra, Figure 5) and from the fitting below 15 K of the susceptibility in the easy direction of **1** by an Ising model.[9] On a single crystal of **1**, the D value of −2.49 K was recently obtained using high field magnetization measurements at 1.5 K with an applied magnetic field in the transverse direction of the chain axis (easy axis).[25,30] It must be pointed out that the D value measured with this technique is, favorably, in good agreement with the estimation reported for $[Mn_2(saltmen)_2(H_2O)_2](ClO_4)_2$ and its derivatives ($D_{Mn}/k_B = -0.55$ to -3.64 K,

(23) Chamberlin, R. V.; Mozurkewich, G.; Orbach, R. *Phys. Rev. Lett.* **1984**, *52*, 867. De Dominics, C.; Orland, H.; Lainée, F. *J. Phys., Lett.* **1985**, *46*, L-463. Weiss, G. H.; Dishon, M.; Long, A. M.; Bendler, J. T.; Jones, A. A.; Inglefield, P. T.; Bandis, A. *Polymer* **1994**, 35, 1880.
(24) Considering the following Hamiltonian, $H = -2J'\sum_i S_{zi}S_{z(i+1)}$, which is equivalent to $H = -2J'S^2\sum_i \sigma_{zi}\sigma_{z(i+1)}$ with $\sigma_i = \pm 1$.
(25) Coulon, C.; Wernsdorfer W.; Clérac, R.; Lecren, L.; Miyasaka, H. Manuscript in preparation.
(26) Loveluck, J. M.; Lovesey, S. W.; Aubry, S. *J. Phys. C: Solid State Phys.* **1975**, *8*, 3841−3856.
(27) Sangregorio, C.; Ohm, T.; Paulsen, C.; Sessoli, R.; Gatteschi, D. *Phys. Rev. Lett.* **1997**, *78* (24), 4645−4648. Hendrickson, D. N.; Christou, G.; Hidehiko, I.; Yoo, J.; Brechin, E. K.; Yamaguchi, A.; Rumberger, E. M.; Aubin, S. M. J.; Sun, Z.; Aromi, G. *Polyhedron* **2001**, *20*, 1479−1488.
(28) Indeed from eq 7, $1/T_B$ can be written $1/T_B = -(k_B/\Delta)(\ln(2\pi\nu_{ac}) + \ln(\tau_0))$
(29) On the basis of the following relation, $J_i = J' + 4J''$, and taking into account that J'' is most likely antiferromagnetic, J_i is the lower limit of J'.
(30) D has been estimated from the relation $2DS^2 \approx g\mu_B SH_a$: Barbara, B.; Thomas, L.; Lionti, F.; Chiorescu, I.; Sulpice, A. *J. Magn. Magn. Mater.* **1999**, *200*, 167−181.

where D_{Mn} is defined as the zero-field splitting of Mn^{III} single ion).[14b] As $J'/k_B = +0.7$ K and the measured anisotropy $D/k_B = -2.49$ K, the calculated energy gap is, therefore, 72.8 K for **1**. This result is in remarkable agreement with the measured energy gap deduced from the Arrhenius behavior shown Figure 10 and definitely validates the single-chain magnet behavior of these series of compounds in the frame of Glauber's theory.

Conclusion

One-dimensional systems have been studied during past decades, but this is only in the most recent two years that experimental examples of single-chain magnet behavior been reported.[9,10] In this paper, we have described synthesis, crystal structures, and magnetic properties of the first series of $Mn^{III}-Ni^{II}$ heterometallic chains, $[Mn_2(saltmen)_2Ni(pao)(L)_2](A)_2$, which behave as single-chain magnets. Substitution of counteranions and ligands has been successfully performed and proved the great stability of their low temperature SCM behavior. Indeed, despite of compounds **1**−**7** having different interchain environments, all parameters related to slow relaxation processes are very similar across the series. This important result emphasizes the one-dimensional nature of this family of compounds and the negligible interchain magnetic interaction which seems to play a minor role in this system in the observed single-chain magnetic behavior. The possibility to further chemically modify the one-dimensional structure of these materials opens new attractive routes of research. Our current efforts are devoted to increasing the interchain interaction to find a crossover between three-dimensional order and SCM behavior but also to increasing the energy gap Δ to be able to raise the blocking temperature. Therefore, we are currently working to change the building blocks constituting the chain and their anisotropy but also to enhance the magnetic interaction between them to increase the blocking temperature.

Experimental Section

General Procedures and Materials. All chemicals and solvents used during the syntheses were reagent grade. The starting material $[Mn_2(saltmen)_2(H_2O)_2](ClO_4)_2$ was synthesized as described elsewhere,[14b] and the other derivatives with different counteranions were synthesized in a similar way. The series of $Ni(pao)_2(L)_2 \cdot n$(solvent) precursors (pao^- = pyridine-2-aldoximate, L = pyridine (py), 4-picoline (4-pic), 4-*tert*-butylpyridine (4-*t*-Bupy), and *N*-methylimidazole (*N*-Meim)) was prepared according to the literature method.[31] The synthesis of **1** was already described in our initial work.[9] *Caution: Perchlorate salts are potentially explosive and should only be handled in small quantities.*

Syntheses of 2−7. Synthetic procedures are almost identical for all materials. Therefore, the synthesis of **2** will be described as a general example. To a solution of $[Mn_2(saltmen)_2(H_2O)_2](ClO_4)_2$ (124 mg, 0.125 mmol) in 10 cm^3 of methanol was added a solution of $Ni(pao)_2(4\text{-pic})_2 \cdot 2CHCl_3$ (181 mg, 0.25 mmol) in 10 cm^3 of methanol. After stirring for 30 min at room temperature, the dark brown solution was diluted with 20 cm^3 of water. The resulting solution was filtered and allowed to stand for 2−3 days to form dark brown crystals of $[Mn_2(saltmen)_2Ni(pao)_2(4\text{-pic})_2](ClO_4)_2$. They were collected by suction filtration, washed with a minimum amount of water, and dried in vacuo. For **3** and **4**, $Ni(pao)_2(4\text{-}t\text{-Bupy})_2$ (143 mg, 0.25 mmol) and $Ni(pao)_2(N\text{-Meim})_2$ (116 mg, 0.25 mmol) have been used, respectively, instead of $Ni(pao)_2(4\text{-pic})_2 \cdot 2CHCl_3$. For **5**−**7**, Mn(III) dimeric units with desired counteranion $[Mn_2(saltmen)_2(H_2O)_2](A)_2$ (A = BF_4^-, 121 mg; PF_6^-, 140 mg; ReO_4^-, 157 mg) have been used with $Ni(pao)_2(py)_2$. For $\mathbf{2} \cdot H_2O$, yield: 68%, 124 mg (based on Mn ion). Anal. Calcd for $C_{64}H_{70}N_{10}O_{15}Cl_2Mn_2Ni$: C, 52.69; H, 4.84; N, 9.60. Found: C, 52.67; H, 4.77; N, 9.79. IR(KBr): ν(C≡N), 1601 cm^{-1}; ν(Cl−O), 1092, 1146, 1130 cm^{-1}. For $\mathbf{3} \cdot 2H_2O$, yield: 85%, 166 mg (based on Mn ion). Anal. Calcd for $C_{70}H_{84}N_{10}O_{16}Cl_2Mn_2Ni$: C, 53.86; H, 5.42; N, 8.97. Found: C, 53.74; H, 5.68; N, 8.96. IR(KBr): ν(C≡N), 1603 cm^{-1}; ν(Cl−O), 1096, 1123, 1146 cm^{-1}. For **4**, yield: 82%, 145 mg (based on Mn ion). Anal. Calcd for $C_{60}H_{66}N_{12}O_{14}Cl_2Mn_2Ni$: C, 50.80; H, 4.72; N, 11.85. Found: C, 50.57, H, 4.72; N, 11.78. IR(KBr): ν(C≡N), 1603 cm^{-1}; ν(Cl−O), 1093, 1123, 1146 cm^{-1}. For $\mathbf{5} \cdot H_2O$, yield: 62%, 109 mg (based on Mn ion). Anal. Calcd for $C_{62}H_{66}N_{10}O_7B_2F_8Mn_2Ni$: C, 52.99; H, 4.73; N, 9.97. Found: C, 53.28; H, 4.71; N, 10.07. IR(KBr): ν(C≡N), 1603 cm^{-1}; ν(B−F), 1036, 1059, 1084 cm^{-1}. For **6**, yield: 75%, 141 mg (based on Mn ion). Anal. Calcd for $C_{62}H_{64}N_{10}O_6P_2F_{12}Mn_2Ni$: C, 49.52; H, 4.29; N, 9.31. Found: C, 49.05; H, 4.24; N, 9.31. IR(KBr): ν(C≡N), 1603 cm^{-1}; ν(P−F), 799, 843, 907 cm^{-1}. For **7**, yield: 92%, 197 mg (based on Mn ion). Anal. Calcd for $C_{62}H_{64}N_{10}O_{14}Mn_2NiRe_2$: C, 43.44; H, 3.76; N, 8.17. Found: C, 43.03; H, 3.82; N, 8.17. IR(KBr): ν(C≡N), 1601 cm^{-1}; ν(Re−O), 908 cm^{-1}.

Physical Measurements. Infrared spectra were measured on KBr disk with a Shimadzu FT-IR-8600 spectrophotometer. Magnetic susceptibility measurements were obtained with the use of a Quantum Design SQUID magnetometer MPMS-XL. The dc measurements were collected from 1.9 to 300 K and from −70 to 70 kOe. The ac measurements were performed at various frequencies from 1 to 1500 Hz with an ac field amplitude of 1 Oe or 3 Oe and no dc field applied. For all the compounds (**1**−**7**), the measurements were performed on finely grounded polycrystalline samples. Experimental data were also corrected for the sample holder and for the diamagnetic contribution calculated from Pascal constants.[32] Hysteresis loops on a single crystal were performed with an array of micro-SQUIDs.[33] This magnetometer works in the temperature range between 0.03 and ∼7 K and in fields up to 1.4 T with sweeping rates as high as 1 T/s, along with a field stability better than a microtesla. The time resolution is about 1 ms. The field can be applied in any direction of the micro-SQUID plane with a precision much better than 0.1° by separately driving three orthogonal coils. In order to ensure a good thermalization, the crystal of about $30 \times 10 \times 5$ μm^3 was fixed by using Apiezo grease. The transverse field magnetization measurements were performed with a home-built Hall probe magnetometer. The Hall probes (typically 10×10 μm^2) are made of two-dimensional GaAs/GaAsAl heterostructures. They work in the temperature range between 1.5 and 100 K, and magnetic fields up to 16 T.

Crystallography. X-ray powder diffraction patterns were collected using Philips PW1820/1710 powder diffractometer with Bragg−Brentano geometry (Cu rotating anode, $\lambda_{K\alpha} = 1.5418$ Å). For single-crystal X-ray crystallography, single crystals of **4**, **6**, and **7** were prepared by the methods described in the synthetic procedure. Single crystals with dimensions $0.12 \times 0.10 \times 0.04$

(31) Crause, R. A.; Busch, D. H. *J. Am. Chem. Soc.* **1960**, *82*, 4830−4834.

(32) Boudreaux, E. A.; Mulay, L. N. *Theory and Applications of Molecular Paramagnetism*; John Wiley & Sons: New York, 1976.

(33) Wernsdorfer, W. *Adv. Chem. Phys.* **2001**, *118*, 99.

mm^3 for **4**, 0.15 × 0.13 × 0.10 mm^3 for **6**, and 0.20 × 0.18 × 0.10 mm^3 for **7** were mounted on a glass rod. Data collections for **4** and **7** were made on a Rigaku CCD diffractometer (Mercury), and the data set for **6** was collected on a Rigaku imaging plate diffractometer (Raxis Rapid). Both diffractometers are used with graphite monochromated Mo Kα radiation ($\lambda = 0.71069$ Å). The structures were solved by a direct method (SIR92)[34] and expanded using Fourier techniques.[35] The non-hydrogen atoms were refined anisotropically, while hydrogen atoms were introduced as fixed contributors. Full-matrix least-squares refinements on F^2 based on 7085 for **4**, 7107 for **6**, and 7082 for **7** unique reflections were employed, where the unweighted and weighted agreement factors of $R = \sum||F_o| - |F_c||/\sum|F_o|$ ($I > 2.00\sigma(I)$) and $R_w = [\sum w(F_o^2 - F_c^2)^2/\sum w(F_o^2)^2]^{1/2}$ were used ($w = 1/[pF_o^2 + 1.0000\sigma_c^2(F_o) + 0.5000]/(4F_c^2)$, $p = 0.001$ for **4**; 0.0007 for **6**; 0.0001 for **7**). A Sheldrick weighting scheme was used. Plots of $\sum w(F_o^2 - F_c^2)^2$ versus F_o^2, reflection order in data collection, sin θ/λ, and various classes of indices showed no unusual trends. Neutral atom scattering factors were taken from Cromer and Waber.[36] Anomalous dispersion effects were included in F_{calcd}; the values $\Delta f'$ and $\Delta f''$ were those of Creagh and McAuley.[37] The values for the mass attenuation coefficients are those of Creagh and Hubbel.[38] All calculations were performed using the CrystalStructure crystallographic software package.[39] In compound **4**, the presence of complicated disorder on parts of *N*-methylimidazole and perchlorate counteranions made difficult the refinement of the structure and the improvement of the *R* factor. Thus, atoms constituting the *N*-methylimidazole part and perchlorate ion were refined isotropically.

Crystal and experimental data for **4**: $C_{60}H_{66}N_{12}O_{14}Cl_2Mn_2Ni$, Ffw = 1418.74, monoclinic *C*2/*c* (No. 15), $T = 123 \pm 1$ K, $a = 21.029(13)$ Å, $b = 15.978(10)$ Å, $c = 18.630(11)$ Å, $\beta = 98.063(9)°$, $V = 6197.9(66)$ Å^3, $Z = 4$, $D_{calcd} = 1.520$ g·cm^{-3}, $F_{000} = 2936.00$, θ range for data collection 3.1−27.5. Final $R = 0.108$, $R_w = 0.255$, GOF = 1.078 for 401 parameters and a total of 24613 reflections, 7085 unique ($R_{int} = 0.095$), of which 3407 with $I > 2.00\sigma(I)$; equivalent reflections were merged. The linear absorption coefficient, μ, for Mo Kα radiation is 0.864 mm^{-1}. An empirical absorption correction was applied which resulted in transmission factors ranging from 0.78 to 1.00. The data were corrected for Lorentz and polarization effects. Max positive and negative peaks in ΔF map were found to be $\rho_{max} = 3.41$ e/Å^3 and $\rho_{min} = -2.69$ e/Å^3.

Crystal and experimental data for **6**: $C_{62}H_{64}N_{10}O_6F_{12}P_2Mn_2Ni$, fw = 1503.76, monoclinic *C*2/*c* (#15), $T = 103 \pm 1$ K, $\lambda = 0.71069$ Å, $a = 21.173(3)$ Å, $b = 16.097(1)$ Å, $c = 19.024(2)$ Å, $\beta = 98.946(4)°$, $V = 6404.9(1)$ Å^3, $Z = 4$, $D_{calcd} = 1.559$ g·cm^{-3}, $F_{000} = 3080.00$, θ range for data collection 3.2−27.5. Final $R = 0.060$, $R_w = 0.132$, GOF = 1.014 for 431 parameters and a total of 28305 reflections, 7107 unique ($R_{int} = 0.090$), of which 4889 with $I > 2.00\sigma(I)$; equivalent reflections were merged. The linear absorption coefficient, μ, for Mo Kα radiation is 0.824 mm^{-1}. An empirical absorption correction based on azimuthal scans of several reflections was applied which resulted in transmission factors ranging from 0.56 to 0.92. The data were corrected for Lorentz and polarization effects. Max positive and negative peaks in ΔF map were found to be $\rho_{max} = 1.62$ e/Å^3 and $\rho_{min} = -1.50$ e/Å^3.

Crystal and experimental data for **7**: $C_{62}H_{64}N_{10}O_{14}Mn_2NiRe_2$, fw = 1714.24, monoclinic *C*2/*c* (No. 15), $T = 123 \pm 1$ K, $\lambda = 0.71069$ Å, $a = 20.860(9)$ Å, $b = 16.010(6)$ Å, $c = 18.732(8)$ Å, $\beta = 98.115(6)°$, $V = 6193.3(43)$ Å^3, $Z = 4$, $D_{calcd} = 1.838$ g·cm^{-3}, $F_{000} = 3384.00$, θ range for data collection 3.2−27.5. Final $R = 0.055$, $R_w = 0.143$, GOF = 0.987 for 537 parameters and a total of 26068 reflections, 7082 unique ($R_{int} = 0.067$), of which 4789 with $I > 2.00\sigma(I)$; equivalent reflections were merged. The linear absorption coefficient, μ, for Mo Kα radiation is 4.666 mm^{-1}. An empirical absorption correction was applied which resulted in transmission factors ranging from 0.74 to 1.00. The data were corrected for Lorentz and polarization effects. Max positive and negative peaks in ΔF map were found to be $\rho_{max} = 4.31$ e/Å^3 and $\rho_{min} = -5.03$ e/Å^3.

Crystallographic data (excluding structure factors) for structures reported in this paper have been deposited at the Cambridge Data Centre as supplementary publication nos. CCDC-210094 for **4**, 210095 for **6**, and 210096 for **7**. Copies of the data can be obtained free of charge on application to CCDC, 12 Union Road, Cambridge CB21EZ, U.K. (Fax: (+44) 1223-336-033. E-mail: deposit@ccdc.cam.ac.uk.)

Acknowledgment. We thank Dr. S. Pechev (ICMCB Pessac, France) for his help in collecting powder X-ray diffraction data, and thank Dr. Kunihisa Sugimoto (X-ray Laboratory, Rigaku Co. Ltd., Japan) for his help and discussion on single-crystal X-ray crystallography. We also acknowledge Dr. B. Barbara (LLN Grenoble, France), Dr. R. Giraud (LLN Grenoble, France), and Dr. Motohiro Nakano (Osaka University, Japan) for their helpful discussion regarding theoretical consideration. H.M. is grateful for financial support from the PRESTO project, Japan Science and Technology Agency (JST), Tokuyama Science and Technology Foundation, and a Grant-in-Aid for Scientific Research from the Ministry of Education, Culture, Sports, Science, and Technology, Japan. M.Y. acknowledges the CREST project, Japan Science and Technology Agency (JST). R.C. and C.C. would like to thank the CNRS and the Conseil Regional d'Aquitaine for financial support. The Université de Bordeaux I is also acknowledged for funding the scientific stay of H.M. in November, 2002.

Supporting Information Available: Crystallographic data in CIF format. This material is available free of charge via the Internet at http://pubs.acs.org.

IC034872O

(34) SIR92: Altomare, A.; Burla, M. C.; Camalli, M.; Cascarano, M.; Giacovazzo, C.; Guagliardi, A.; Polidori, G. *J. Appl. Crystallogr.* **1994**, *27*, 435.

(35) DIRDIF94: Beurskens, P. T.; Admiraal, G.; Beurskens, G.; Bosman, W. P.; de Gelder, R.; Israel, R.; Smits, J. M. M., 1994.

(36) Cromer, D. T.; Waber, J. T. *International Tables for Crystallography*; The Kynoch Press: Birmingham, England, 1974; Vol IV, Table 2.2A.

(37) Creagh, D. C.; McAuley, W. J. *International Tables for Crystallography*; Wilson, A. J. C., Ed.; Kluwer Academic Publishers: Boston, 1992; Vol C, Table 4.2.6.8, pp 219−222.

(38) Creagh, D. C.; Hubbell, J. H. *International Tables for Crystallography*; Wilson, A. J. C., Ed.; Kluwer Academic Publishers: Boston, 1992; Vol C, Table 4.2.4.3, pp 200−206.

(39) *CrystalStructure 3.15: Crystal Structure Analysis Package*; Rigaku and Rigaku/MSC9009: The Woodlands, TX, 2000−2002.